Corrosion Inhibition of mild steel in hydrochloric acid solution by pyrido[2,3-b]pyrazine derivative: electrochemical and theoretical evaluation

M. Y. Hjouji[1], M. Djedid[5], H. Elmsellem[2]*, Y. Kandri Rodi[1]*, Y. Ouzidan[1], F. Ouazzani Chahdi[1], N. K. Sebbar[3], E. M. Essassi[3], I. Abdel-Rahman[4], B. Hammouti[2]

[1]*Laboratory of Applied Organic Chemistry, Faculty of Science and Technology, Sidi Mohammed Ben Abdellah University, Fez, Morocco.*
[2]*LC2AME, Faculté des Sciences, University Mohammed Premier, B.P. 717, 60000 Oujda, Morocco.*
[3]*Laboratoire de Chimie Organique Hétérocyclique, URAC 21, Pôle de Compétences Pharmacochimie, Université Mohammed V, Faculté des Sciences, Av. Ibn Battouta, BP 1014 Rabat, Morocco.*
[4]*Department of Chemistry, College of Arts & Sciences, University of Sharjah, PO Box: 27272, UAE.*
[5]*Laboratory of process engineering, Department Process Engineering, Laghouat University, P.O Box 37G, Route de Ghardaïa, 03000, Laghouat, Algeria.*

Abstract

In this paper, the synthesis and the corrosion inhibition efficiency of pyrido[2,3-b]pyrazine derivative (P1) on mild steel in acidic media were studied. Corrosion inhibition effect of (P1) on mild steel in 1 M HCl solution was investigated using weight loss measurements, electrochemical polarization and electrochemical impedance spectroscopy (EIS) methods. Results obtained reveal that P1 acts as a mixed inhibitor without modifying the hydrogen reduction mechanism. The inhibition efficiency increases with the increase of the concentration of (P1) reaches a maximum value of 93% at 10-3M. The inhibition efficiency of (P1) decreases with the rise of temperature. It was found that (P1) adsorbed on the mild steel surface according to Langmuir isotherm model. Quantum chemical studies were also carried out to propose an interpretation of the data.

Keywords: corrosion inhibition, pyrido[2,3-b]pyrazine, weight loss, polarization, adsorption, DFT.

1. Introduction

The pharmacological and therapeutic activities that present a variety of heterocyclic molecules containing a pyrido[2,3-b] pyrazine pattern, have greatly aroused the interest of researchers for the development of new routes to such compounds. It should be noted that the system pyrido[2,3-b] pyrazine is well known by its photophysical [1], antibacterial [2] anti-inflammatory [3] and anti-cancer properties [4]. More recently, studies have shown that pyridopyrazinone derivatives are good stimulators of insulin secretion, and therefore they can be used for treatment of diabetes [5]. The reactivity of allyl bromide towards 7-bromopyrido[2,3-b]pyrazine-2,3(1H,4H)-dione under phase-transfer catalysis conditions using tetra n-butyl ammonium bromide (TBAB) as catalyst and potassium carbonate as base, leads to the formation of the title compound (P1) in good yield (**Scheme 1**). Several classes of organic compounds like pyridopyrazine derivative are broadly used as corrosion inhibitors for metals in acid environments, since they possess the nitrogen and oxygen atoms which can easily be protonated to exhibit good inhibitory action on the corrosion of metals [6-7].

The purpose of the present study is to evaluate the corrosion inhibition efficiency of the synthesized compound (P1) on mild steel in 1 M hydrochloric acid solution, (**Scheme 1**).

In addition to that, to extend these investigations in order to obtain a better understanding of the mode of inhibitory action of (P1) by calculating theoretical parameters for both mild steel dissolution and inhibitor adsorption process in hydrochloric acid solution using DFT and electrochemical methods.
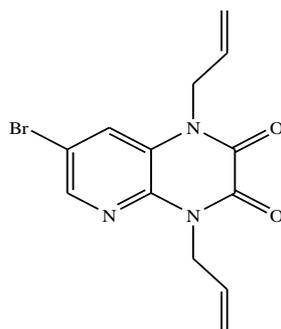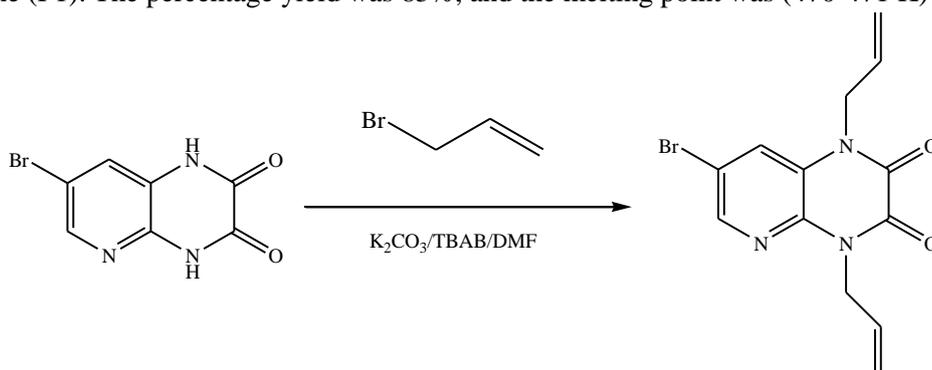
Scheme 1: 1,4-diallyl-7-bromopyrido[2,3-b]pyrazine-2,3(1H,4H)-dione **(P1)**.

2. Experimental details

2.1. Synthesis of inhibitors

In a flask equipped with a magnetic stirrer, 7-bromopyrido [2,3-b] pyrazine-2,3 (1H, 4H) -dione (1 mmol, 0.25g), 20ml of DMF, potassium carbonate K_2CO_3 (2.1 mmol, 0.29g), tétra-n-butylammonium bromide (TBAB) (0.2 mmol, 0.064g) were mixed and stirred for 5 min; Then, 0.18 ml of allyl bromide (2 mmol) was added dropwise to the reaction mixture. The reaction was brought at room temperature for 6 hours. After removal of salts by filtration, the DMF was evaporated under reduced pressure and the residue obtained was dissolved in dichloromethane. The rest of the salts were removed by washing the organic phase three times with distilled water. Concentrated to dryness, the compound desired was purified by flash column chromatography (on silica-gel with ethyl acetate: hexane, 1:1) to afford a white solid 1,4-diallyl-7-bromopyrido[2,3-b]pyrazine-2,3(1H,4H)-dione (P1). The percentage yield was 85%, and the melting point was (470-471 K) (**Scheme 2**):

Scheme 2: Synthesis of 1,4-diallyl-7-bromopyrido[2,3-b]pyrazine-2,3(1H,4H)-dione (P1).

The analytical and spectroscopic data are conforming to the structure of compounds formed:

(P1): Yield = 85%; M.p. 470-471 K; **NMR ^{1}H δppm**: 8.29 (d, 1H, H pyr, J=1.8 Hz); 7.60 (d, 1H, H pyr, J=1.8 Hz); 5.83-6.037 (m, 2H, -CH =); 5.208-5.374 (m, 4H, =CH$_2$); 5.008 (dd$_{trip}$ 2H, -N-CH$_2$) ; 4.824 (dd$_{trip}$, 2H,-N-CH$_2$); **NMR ^{13}C δppm***: 153.78, 153.251 (C=O); 143.189, 134.906 (-CH pyr); 137.415, 123.849 (Cq); 130.692, 129.435 (-CH =); 119.096 (2 =CH$_2$); 114.56 (-C-Br); 45.287, 44.166 (2 N-CH$_2$).

2.2. Solutions

The aggressive solutions of 1M HCl were prepared by dilution of an analytical grade 37% HCl with double distilled water. Different concentrations of the inhibitor (P1) (10^{-6} - 10^{-3} M) were prepared by stirring the appropriate amount of (P1) in 100 ml of 1 M HCl at room temperature. The 100 ml of 1 M HCl solution without inhibitor was used as blank test.

2.3. Preparation of Specimens

The mild steel sheets were cut into $2.00 \times 2.00 \times 0.25$ cm^3 dimensions with the following composition:

Composition	**P**	**Al**	**Si**	**Mn**	**C**	**S**	**Fe**
	0.09%	0.01%	0.38%	0.05%	0.21%	0.05%	Balance

The above sheets were used for weight loss measurements. Prior to all measurements, the sheets surfaces were abraded with 180, 400, 800, 1000, 1200 grades of emery papers. The specimens were washed thoroughly with bidistilled water, degreased with ethanol, and dried.

2.4. Weight Loss Method
Gravimetric measurements of square steel specimens of size 2 x 2 x 0.25 cm^3 in 1 M HCl with and without addition of different concentrations of the inhibitor (P1). The corrosion rate was determined after 6 h of immersion period, at a temperature of 308K by the following equation:

$$\vartheta = \frac{\Delta m}{S \times t} \qquad (1)$$

Where: Δm is the average weight loss, *S* the total area, and *t* is the immersion time.

2.5. Electrochemical Measurements:
Electrochemical experiments were recorded using potentiostat PGZ 100 piloted by Volta master soft ware; the electrochemical measurements were carried out in conventional three electrode electrolysis cylindrical Pyrex glass cell. The working electrode (WE) has the form of a disc cut from the steel sheet, the area exposed to the corrosive 1 M HCl solution was 1 cm^2. A satured calomel electrode (SCE) and a platinum electrode were used respectively as reference and auxiliary electrodes. The temperature of the cell was controlled by using a thermostat at 308 K. The potential must be stabilized for 30 min's. before starting any test.
The inhibition efficiency E_P was defined as:

$$E_p\% = \frac{I°corr - Icorr}{I°corr} \times 100 \qquad (2)$$

Where $I°_{corr}$ and I_{corr} represent corrosion current density values in the absence and presence of the inhibitor, respectively.
The electrochemical impedance spectroscopy (EIS) measurements were carried out with the electrochemical system, which included a digital potentiostat model Voltalab PGZ100 computer at E_{corr} after immersion in solution without bubbling. After the determination of steady-state current at a corrosion potential, sine wave voltage (10 mV) peak to peak, at frequencies between 100 kHz and 10 mHz were superimposed on the rest potential. Computer programs automatically controlled the measurements performed at rest potentials after 0.5 hour of exposure at 308 K. The impedance diagrams were given in the Nyquist representation.
Each experiment was duplicated to check the reproducibility.
The inhibition efficiency E_{Rt} was defined as:

$$E_{Rt}\% = \frac{R°ct - Rct}{R°ct} \times 100 \qquad (3)$$

Where, $R°_{ct}$ and R_{ct} are the charge transfer resistance values in the absence and presence of inhibitor, respectively.

2.6. Quantum chemical calculations
The quantum chemical calculations reported in this work were performed at the B3LYP/6-31G (d,p) level of theory using GAUSSIAN 09 series of programs [8]. The optimizations of equilibrium geometries of all reactants were performed using the Berny analytical gradient optimization method [9-12]. The electronic populations as well as the Fukui indices and local nucleophilicities were computed using different populations analysis MPA (Mulliken population analysis) and NPA (natural population analysis) [13-16]. The cationic systems, needed in the calculation of nucleophilic Fukui indices, were taken in the same geometry as the neutral system.
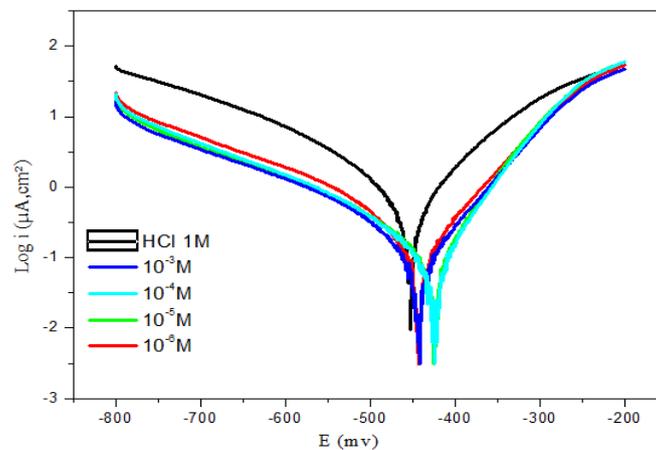
3. Results and Discussion
3.1. Potentiodynamic Polarization Measurements
The Potentiodynamic polarization curves for mild steel in 1 M HCl without and with various concentrations of the inhibitor (P1) are shown in (**Figure 1**). It is apparent from (**Figure 1)** that the polarization curves shifted to lower current regions in the presence of the inhibitor compared to the blank sample. This suggests that the synthesized compound (P1), reduces the corrosion current density, which is an indication of its corrosion inhibition potential. The polarization curve in the presence of 10^{-3}M concentration of (P1) appears at relatively more cathodic potential compared to the blank sample, while the curves appear at relatively more anodic potentials at higher concentrations of (P1).

This suggests that the inhibitive effect of (P1) is more cathodic at 10^{-3} M than at lower concentrations. The electrochemical kinetic parameters obtained from the Tafel extrapolations are listed in (**Table 1**). It is clearly evident from the results in (**Table 1**) that the maximum shift in the E_{corr} in the presence of the inhibitor relative to the HCl is observed at 10^{-6} M of (P1) (-464 mV and -455 mV).

An inhibitor can be classified as a cathodic or anodic inhibitor only if the displacement in E_{corr} is greater than 85 mV; otherwise, it is a mixed-type inhibitor [17-18]. The slight shift in E_{corr} in the present study implies that the studied inhibitor (P1) is a mixed-type inhibitor, which means that (P1), retards both the anodic dissolution of mild steel in HCl and the cathodic hydrogen ion reduction process. The values of the Tafel slopes βc changed with change in concentration of the inhibitor. This suggests that the rate of the corrosion reaction of mild steel in the acidic media is affected by the change in concentration of the inhibitor.

In other words, the inhibitor (P1) is a mixed type inhibitor with predominantly cathodic inhibitive effects. The corrosion current density decreases with increasing concentration of the inhibitor, which is also an indication of the inhibitive effect of (P1). The values of the percentage inhibition efficiency (%Ep) also revealed that the inhibition efficiency increases with increasing concentration of (P1).

Figure 1. Potentiodynamic polarization curves for mild steel in 1 M HCl without and with various concentrations of the inhibitor (P1).

Table 1. Tafel parameters for mild steel corrosion in 1 M HCl without and with various concentrations of the inhibitor (P1).

Inhibitor	Concentration (M)	E_{corr} (mV/SCE)	I_{corr} ($\mu A/cm^2$)	$-\beta c$ (mV/dec)	E_p %
1 M HCl	--	-455	1386	101	--
inhibitor (P1)	10^{-6}	-470	361	96	74
	10^{-5}	-452	285	87	79
	10^{-4}	-450	209	78	85
	10^{-3}	-464	133	92	90

3.2. Electrochemical impedance spectroscopy measurements:

The corrosion behavior of steel, in acidic solution in the absence and presence of the inhibitor (P1), was also investigated by EIS method at 308 K after 30 min of immersion (**Figure 2**).

The impedance parameters derived from these investigations are listed in (**Table 2**). From **Figure 2**, the obtained impedance diagrams (almost a semi-circular appearance), indicates that a charge transfer process mainly controls the corrosion of steel [19]. The general shape of the curves is very similar for all samples; the shape is maintained throughout the whole concentration, indicating that almost no change in the corrosion mechanism occurred due to the inhibitor addition [20]. The R_t values increased with the increase of the concentration of (P1). Values of double layer capacitance are also brought down to the maximum extent in the presence of inhibitor and the decrease in the values of C_{dl} follows the order similar to that obtained for I_{corr} in

this study. The results obtained from the polarization technique in acidic solution were in good agreement with those obtained from the electrochemical impedance spectroscopy (EIS) with a small variation.
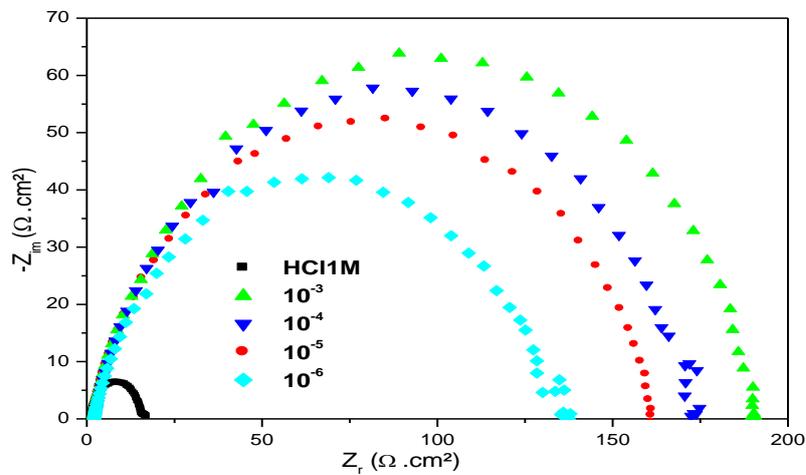
Figure 2. Nyquist plots for mild steel in 1 M HCl containing different concentrations of (P1).

Table 2. AC impedance data of mild steel in 1.0 M HCl acid solution containing different concentrations of (P1) at 308K.

Inhibitor	Concentration (M)	Rt (Ω.cm2)	Cdl ($\mu f/cm^2$)	E_{Rt} (%)
1 M HCl	--	14.7	200	--
Inhibitor P1	10^{-3}	195	110	93
	10^{-4}	170	84	91
	10^{-5}	167	51	90
	10^{-6}	138	47	89

3.3. Weight loss measurements:

Weight loss corrosion tests were carried out on the mild steel in 1M HCl in the absence or presence of (P1) over a period of 6 hours. The corrosion rates values [$mg \cdot cm^{-2} \cdot h^{-1}$] were tabulated in (**Table3**).

The percentage of inhibition was calculated according to the following expression:

$$\eta(\%) = \left(1 - \frac{w_i}{w_o}\right) \cdot 100 \quad \textbf{(4)}$$

where w_0 and w_i are the values of corrosion weight losses of mild steel in uninhibited and inhibited solutions, respectively.

Table 3. Corrosion parameters obtained from weight loss measurements for mild steel in 1 M HCl containing various concentrations of (P1) at 308 K.

Inhibitor	Concentration (M)	C_R ($mg.cm^{-2}h^{-1}$)	η (%)
1 M HCl	--	0.82	--
Inhibitor P1	10^{-6}	0.19	77
	10^{-5}	0.17	79
	10^{-4}	0.11	87
	10^{-3}	0.08	90

It is apparent from (**Table 3**) that the inhibition efficiency increases with the increase of the concentration of (P1) and reaches 90% with a concentration as low as 10^{-3} M of (P1), which shows a good inhibition efficiency for mild steel in aggressive acidic solutions of 1 M hydrochloric acid.

J. Mater. Environ. Sci. 7 (4) (2016) 1425-1435
ISSN : 2028-2508
CODEN: JMESCN

M. Y. Hjouji et al.

3.4. Adsorption Isotherm:

The inhibition of metal corrosion by organic molecules is usually as a result of adsorption of the inhibitor molecules on the metal surface. Therefore, an insight into the inhibition mechanism can be gained from the adsorption isotherm. The adsorption of an organic adsorbate onto metal–solution interface can be represented by a substitution adsorption process between the organic molecules in the aqueous solution phase (Org(sol)) and the water molecules on the metallic surface ($H_2O_{(ads)}$) according to the equation:

$$\textbf{Org}_{\textbf{(sol)}} + x\ \textbf{H2O}_{\textbf{(ads)}} \longrightarrow \textbf{Org}_{\textbf{(ads)}} + x\ \textbf{H2O}_{\textbf{(sol)}} \quad \textbf{(5)}$$

Where *x* is the size ratio of the number of water molecules replaced by one molecule of organic substrate. Adsorption isotherms are often employed to gain more insights into the mechanism of corrosion inhibition, due to the fact that thermodynamic adsorption parameters provide information about the mode of interactions between the inhibitor molecules and the active sites on the metal surface [21-23]. The experimental data in the present study were subjected to various adsorption isotherms including Langmuir, Temkin, Freundlich, Frumkin and Flory–Huggins but the Langmuir adsorption isotherm gave the best correlation. Therefore, thermodynamic adsorption parameters for mild steel in 1 M HCl in the presence of the studied inhibitor (P1) were obtained from the Langmuir isotherm plot of the form:

$$C/\theta = 1/K_{ads} + C \quad \textbf{(6)}$$

Where θ is the degree of surface coverage, K_{ads} is the equilibrium constant of the adsorption process and C_{inh} is the concentration of the inhibitor. The Langmuir adsorption isotherm plot is shown in Figure 3, indicating near unity values of slope and correlation coefficient (R^2). The adsorption equilibrium constant, K_{ads}, was obtained from the intercept and the change in Gibb's free energy (ΔG_{ads}) for the adsorption process was obtained using the equation:

$$\Delta G°_{ads} = -RT\ \ln\ (55.5\ K_{ads}) \quad \textbf{(7)}$$

Where R is the universal gas constant, T is absolute temperature and 55.5 is the molar concentration of water in solution. Since the K_{ads} represents the degree of adsorption, a high value of K_{ads} signifies that the inhibitor is strongly adsorbed on the steel surface [24]. The value of 4.73 10^5 l/mol obtained for the K_{ads} in the present study is an indication of strong adsorption of the molecules of (P1) to the steel surface.

The value of ΔG_{ads} is often used to classify the adsorption process as physisorption, chemisorption or a combination of both. Generally, a value of ΔG_{ads} around -20 kJmol^{-1} or less negative suggests that the adsorption process involves electrostatic interactions between the charged molecules and the charged metal surface, termed physisorption, whereas a value of ΔG_{ads} around -40 kJmol^{-1} or more negative indicates the involvement of charge sharing or transfer from organic molecules to the metal surface during the adsorption process leading to the formation of coordinate bond and the adsorption process is termed chemisorption [25]. The value of -43.73 kJmol^{-1} obtained for ΔG_{ads} in the present study probably means that the adsorption of (P1) on the steel surface exhibits chemisorption adsorption.
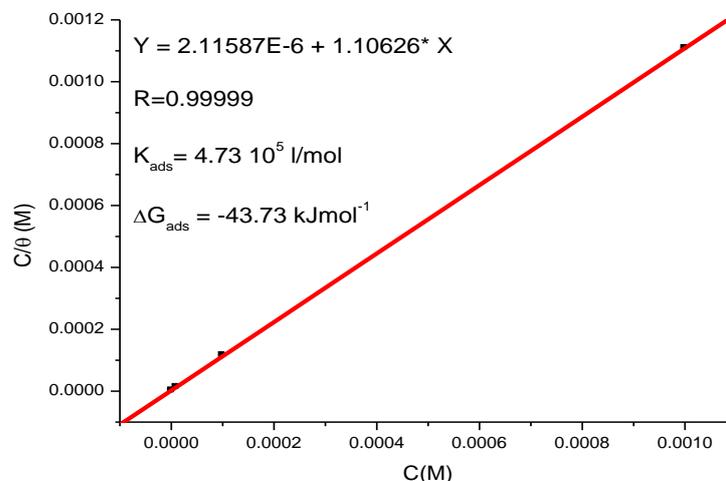
Figure 3. Langmuir adsorption isotherm for mild steel in 1 M HCl containing various concentrations of (P1) at 308 K. The values of K_{ads} and ΔG_{ads} are listed on the graph.

3.5. Theory and computational details
3.5.1.Theoretical background
  ➢ **Global quantities**
Popular qualitative chemical concepts such as electronegativity [26-27] (χ) and hardness [28] (η) have been provided with rigorous definitions within the purview of conceptual density functional theory [29-31] (DFT). Electronegativity is the negative of chemical potential defined [32] as follows for an N-electron system with total energy E and external potential $v(\vec{r})$

$$\chi = -\mu = -\left(\frac{\partial E}{\partial N}\right)_{v(r)} \quad \textbf{(8)}$$

μ is the Lagrange multiplier associated with the normalization constraint of DFT [33].
Hardness (η) is defined [34] as the corresponding second derivative,

$$\eta = -\left(\frac{\partial^2 E}{\partial N}\right)_{v(r)} = -\left(\frac{\partial \mu}{\partial N}\right)_{v(r)} \quad \textbf{(9)}$$

Using a finite difference method, working equations for the calculation of χ and η may be given as [35]:

$$\chi = \frac{I+A}{2} \quad \textbf{(10)}$$

$$\eta = \frac{I-A}{2} \quad \textbf{(11)}$$

Where I and A are the ionization potential and electron affinity, respectively. If E_{HOMO} and E_{LUMO} are the energies of the highest occupied and lowest unoccupied molecular orbitals, respectively, then the above equations can be rewritten, [36] using Koopmans' theorem [37], as

$$\chi = -\frac{E_{HOMO} + E_{LUMO}}{2} \quad \textbf{(12)}$$

$$\eta = -\frac{E_{HOMO} - E_{LUMO}}{2} \quad \textbf{(13)}$$

  ➢ **Local quantities**
Local quantities such as Fukui function f(r) defined the reactivity/selectivity of a specific site in a molecule. The Fukui function is defined as the first derivative of the electronic density q(r) of a system with respect to the number of electrons N at a constant external potential v(r) [38].

$$f(r) = \left[\frac{\partial \rho(r)}{\partial N}\right]_{v(r)} = \left[\frac{\delta \mu}{\delta v(r)}\right]_N \quad \textbf{(14)}$$

Using left and right derivatives with respect to the number of electrons, electrophilic and nucleophilic Fukui functions for a site k in a molecule can be defined [39].

$$f_k^+ = P_k(N+1) - P_k(N) \qquad \text{for nucleophilic attack} \qquad \textbf{(15a)}$$

$$f_k^- = P_k(N) - P_k(N+1) \qquad \text{for electrophilic attack} \qquad \textbf{(15b)}$$

$$f_k^0 = |P_k(N+1) - P_k(N-1)| / 2 \quad \text{for radical attack} \qquad \textbf{(15c)}$$

Where, $P_k(N)$, $P_k(N+1)$ and $P_k(N-1)$ are the natural populations for the atom k in the neutral, anionic and cationic species respectively.
The fraction of transferred electrons ΔN was calculated according to Pearson theory [40]. This parameter evaluates the electronic flow in a reaction of two systems with different electronegativities, in particular case; a metallic surface (Fe) and an inhibitor molecule. ΔN is given as follows:

$$\Delta N = \frac{\chi_{Fe} - \chi_{inh}}{2(\eta_{Fe} + \eta_{inh})} \quad \textbf{(16)}$$

Where χFe and χinh denote the absolute electronegativity of an iron atom (Fe) and the inhibitor molecule, respectively; ηFe and ηinh denote the absolute hardness of Fe atom and the inhibitor molecule, respectively. In order to apply the eq. 18 in the present study, a theoretical value for the electronegativity of bulk iron was

used χFe = 7 eV and a global hardness of ηFe = 0, by assuming that for a metallic bulk IP = EA because they are softer than the neutral metallic atoms [40].

Recently, a new global chemical reactivity parameter has been introduced and known as electrophilicity index (ω) .It is deined as [41].

$$\omega = \frac{\chi^2}{2\eta} \qquad (17)$$

High ionization energy (IE = 6. 9622 eV) indicates high stability, the number of electrons transferred (ΔN) was also calculated and tabulated in (**Table 5**). Because ΔN < 3.6, this means that the inhibitor (P1) has the tendency to donate electrons to the metal surface by chemisorption process [42-43].

Table 4. Calculated quantum chemical parameters of the studied inhibitor(P1) .

Quantum parameters	Inhibitor (P1)
Total energy (eV)	-92215
E $_{HOMO}$ (eV)	-6. 9622
E $_{LUMO}$ (eV)	-0.5404
ΔEgap (eV)	6.4218
μ (debye)	4.1171
IE(eV)	6. 9622
EA(eV)	0.5404
χ(eV)	3.7513
η(eV)	3.2109
ω (eV)	2.1904
ΔN	0.5060

The calculated values of the f^+ for the inhibitor (P1) are mostly localized on the pyridopyrazine ring. Namely C_2, O_{11}, O_{12} and N_{15}, indicating that the pyridopyrazine ring will probably be the favorite site for nucleophilic attack [44].

The results also show that O_{11} and O_{12} atoms are suitable site to undergo both nucleophilic and electrophilic attacks, probably allowing them to adsorb easily and strongly on the mild steel surface.

Table 5. Pertinent natural populations and Fukui functions of the studied inhibitor (P1) calculated at B3LYP/6-31G(d,p) in gas phase:

Atom	N(K)	N(K+1)	N(K-1)	f^+	f	f^0
C $_2$	6,2476	6,3712	6,2357	0,1236	0,0119	0,0678
Br$_{10}$	34,9234	35,0135	34,7659	0,0901	0,1575	0,1238
O$_{11}$	8,5570	8,6688	8,4402	0,1118	0,1169	0,1143
O$_{12}$	8,5618	8,6676	8,4562	0,1058	0,1056	0,1057
N$_{15}$	7,4650	7,5642	7,4422	0,0992	0,0228	0,0610

Table 6. Pertinent natural populations and Fukui functions of the studied inhibitor (P1) calculated at B3LYP/6-31G(d,p) in aqueous phase:

Atom	N(K)	N(K+1)	N(K-1)	f^+	f	f^0
C $_2$	6,2476	6,3220	6,2351	0,0743	0,0125	0,0434
C $_8$	5,3928	5,5274	5,3632	0,1346	0,0297	0,0821
C $_9$	5,3909	5,5236	5,3630	0,1327	0,0279	0,0803
O$_{11}$	8,5570	8,7237	8,4941	0,1666	0,0630	0,1148
O$_{12}$	8,5618	8,7212	8,5026	0,1594	0,0592	0,1093
N$_{15}$	7,4650	7,5414	7,4602	0,0764	0,0049	0,0406
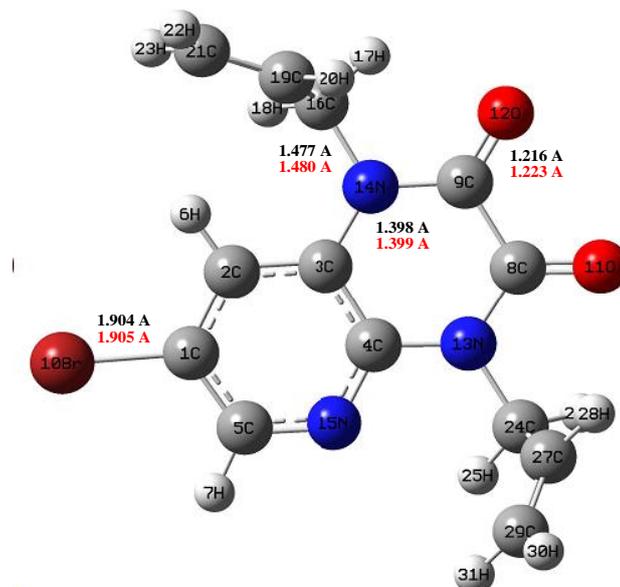
Figure 4. Optimized molecular structures and bond lengths of the studied inhibitor (P1) calculated in gas (black) and aqueous (red) phases at B3LYP/6-31G(d,p) level

After the analysis of the theoretical results, indicates that the inhibitor (P1) contains a non-planar moiety. In fact, the allyl groups are almost perpendicular to the pyridopyrazine core [45].

HOMO (G)

LUMO (G)

HOMO (A)

LUMO (A)
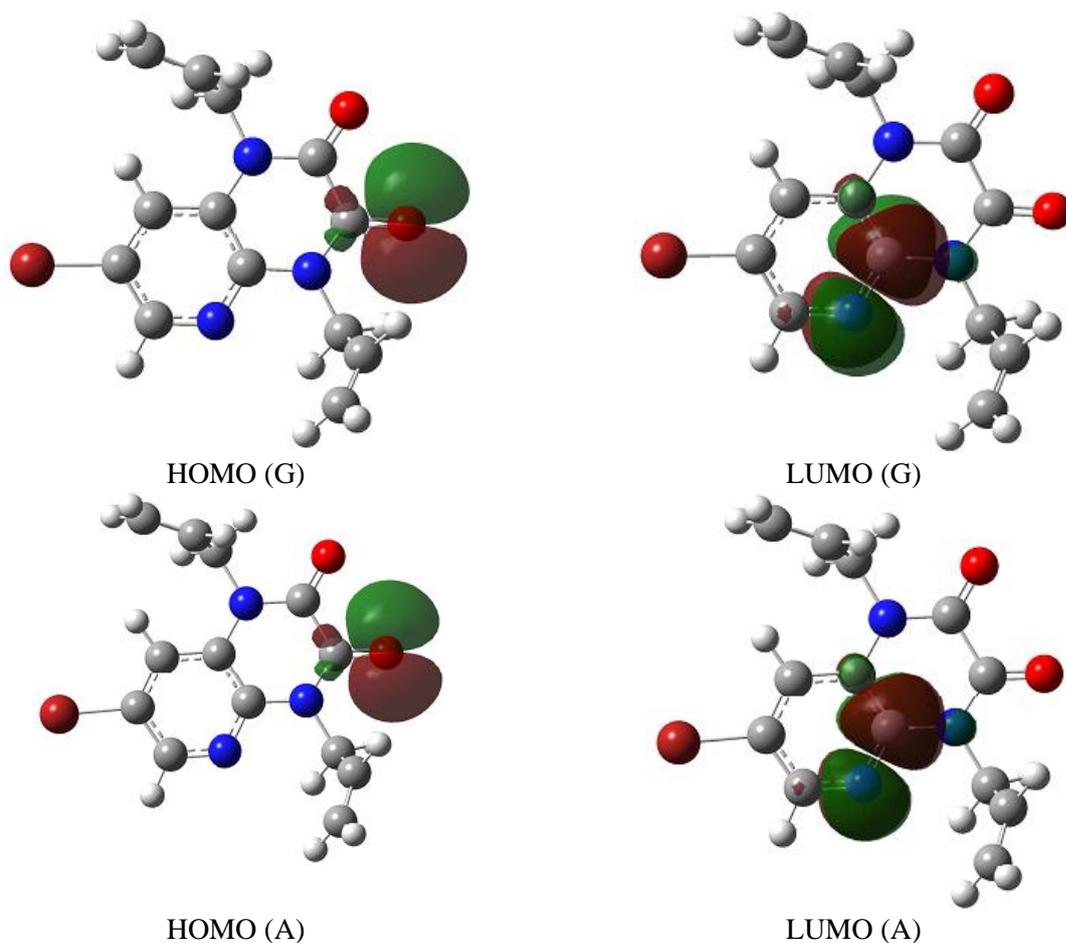
Figure 5 : The HOMO and the LUMO electrons density distributions of the studied inhibitor (P1) at B3LYP/6-31G(d,p) level in gas and aqueous phases.

Conclusion

From the overall studies, the following conclusions could be deduced:
- ➢ The three studied methods (weight loss, electrochemical polarization, and electrochemical impedance spectroscopy) showed a good agreement.
- ➢ The studied inhibitor (P1) acts as a mixed inhibitor without modifying the hydrogen reduction mechanism.
- ➢ The inhibition efficiency increases with the increase of concentration of (P1) concentration to attain a maximum value of 93% at 10^{-3}M.
- ➢ EIS measurements show that the charge transfer resistance (Rct) increases and the double layer capacitance (C_{dl}) decreases in the presence of the inhibitor (P1) which implied the adsorption of the inhibitor molecules on the mild steel surface.
- ➢ Adsorption of the tested inhibitor (P1) follows Langmuir adsorption isotherm.
- ➢ Quantum chemical calculations showed a good agreement between the theoretical and experimental results.

Reference

1. Thirumurugan P., Muralidharan D., Perumal P. T., *Dyes and Pigment.s.* 81 (2009)245-253.
2. Miyazawa T., takabatake T. and hasegawa M., *Yakugaku Zasshi.* 117 (2) (1997)126-132**.**
3. Seitz L.E., Suling W.J., Reynolds R.C., *Journal of Medicinal Chemistry.* 45 (2002)5604-6.
4. Burguete A., Pontiki E., Litina D.H., Villar R., Vicente E. & Solano B., *Bioorganic and Medicinal Chemistry Letters.* 17 (2007) 6439-43.
5. Botton G., Valeur E., Kergoat M., Charon C., Elbawab S., Patent No.: US 8,642,617 B2.
6. Niouri W., Zerga B., Sfaira M., Taleb M., Hammouti B., Ebn Touhami M., Al-Deyab S.S., Benzeid H., Essassi E. M.. *J. Electrochem. Sci*. (2012) 10190-10204.
7. Thomas J.G.N., *Symp. Corros. Inhibitors*. (1981), 453.
8. Elmsellem H., Youssouf M. H., Aouniti A., Ben Hadd T., Chetouani A., Hammouti B., *Journal of Applied Chemistry.,* 87(6) (2014) 744−753.
9. Elmsellem H., Aouniti A., Khoutou M., Chetouani A., Hammouti B., Benchat N., Touzani R. and Elazzouzi M., *J. Chem. Pharm. Res.,* 6 (2014) 1216.
10. Elmsellem H., Harit T., Aouniti A., Malek F., Riahi A., Chetouani A., Hammouti B., *Protection of Metals and Physical. Chemistry of Surfaces,* 51(5) (2015)873.
11. Elmsellem H., Aouniti A., Youssoufi M.H., Bendaha H., Ben hadda T., Chetouani A., Warad I., Hammouti B., *Phys. Chem. News*., 70 (2013) 84.
12. Elmsellem H., Elyoussfi A., Steli H., Sebbar N. K., Essassi E. M., Dahmani M., El Ouadi Y., Aouniti A., El Mahi B., Hammouti B., *Der Pharma Chemica*., 8(1) (2016) 248-256.
13. Li J., Li H., Jakobsson M., Li S., Sjodin P., Lascoux M., *Mol. Ecol*., 21 (2012)28.
14. Yamamoto K., Irimura T., *J. Biochem*., 150 (2011) 477.
15. Zhao X., Wang Y., Chen Q., Zhang M., Zhao N., *Comput, Mater. Sci*., 54 (2012)119.
16. Balachandran V., Lakshmi A., Janaki A., *J. Mol. Struct*., 395 (2011) 1006.
17. Aouniti A., Elmsellem H., Tighadouini S., Elazzouzi M., Radi S., Chetouani A., Hammouti B., Zarrouk A., *Journal of Taibah University for Science.*, (2015), http://dx.doi.org/10.1016/j.jtusci.2015.11.008.
18. Elmsellem H., Karrouchi K., Aouniti A., Hammouti B., Radi S., Taoufik J., Ansar M., Dahmani M., Steli H. and El Mahi B., *Der Pharma Chemica*. 7(10)(2015)237-245.
19. Elmsellem H., Nacer H., Halaimia F., Aouniti A., Lakehal I., Chetouani A ., Al-Deyab S. S., Warad I., Touzani R., Hammouti B.. *Int. J. Electrochem. Sci.*, 9 (2014) 5328.
20. Elmsellem H., Basbas N., Chetouani A., Aouniti A., Radi S., Messali M., Hammouti B., *Portugaliae Electrochimica Acta*, 2 (2014) 77.

21. Chakib I., Elmsellem H., Sebbar N. K., Essassi E. M., Fichtali I., Zerzouf A., Ouzidan Y., Aouniti A., El Mahi B. and Hammouti B., *Der Pharma Chemica.*, 8(2) (2016)380-391.

22. Essaghouani A. L., Elmsellem H., Ellouz M., El Hafi M., Boulhaoua M., Sebbar N. K., Essassi E. M., Bouabdellaoui M., Aouniti A. and Hammouti B., *Der Pharma Chemica.*, 8(2) (2016)297-305.

23 Elmsellem H., Harit T., Aouniti A., Malek F., Riahi A., Chetouani A and Hammouti B., *Protection of Metals and Physical Chemistry of Surfaces,* 51(5) *(*2015)873–884.

24. Elmsellem H., Elyoussfi A., Sebbar N. K., Dafali A., Cherrak K., H. Steli, E. M. Essassi, A. Aouniti and B. Hammouti, *Maghr. J. Pure & Appl. Sci.,* 1 (2015) 1-10.

25. Elmsellem H., Bendaha H., Aouniti A., Chetouani A., Mimouni M., Bouyanzer A., *Mor. J. Chem.*, 2 (2014) 1-9.

26. Pauling L., The nature of the chemical bond, 3rd edn. (Cornell University Press, Ithaca, 1960)

27. Sen K.D., Jorgenson C., Springer. Berlin. 66 (1987)

28. Sen K.D., Mingos D.M.P., *Springer.Berlin*.80(1993).

29. Parr R.G., Yang W., Oxford University Press,Oxford. (1989).

30. Geerlings P., Proft F., Langenaeker W., *Chem. Rev*. 103 (2003) 1793.

31. Chermette H., *J. Comput. Chem*. 20 (1999)129.

32. Parr R.G., Donnelly R.A., Levy M., Palke W., *J. Chem. Phys*. 68 (1978)3801.

33. Hohenberg P., *Kohn, Phys. Rev. B*. 136 (1964) 864 .

34. Parr R.G., Pearson R.G., *J. Am. Chem. Soc*., 105 (1983)7512.

35. Obot I. B. and Obi-Egbedi N. O., *Corrosion Science.* 52 (2) (2010) 657.

36. Lucjan P. Elsevier. Oxford. (2007).

37. Parr R.G., Yang W., *J. Am. Chem. Soc*. 106 (1984) 4049.

38. Yang W., Mortier W., *J. Am. Chem. Soc*., 108 (1986) 5708.

39. Roy R.K., Pal S., Hirao K*., J. Chem. Phys.*, 110 (1999) 8236.

40. Pearson R.G., *Inorg. Chem*. 27 (1988) 734.

41. Kabanda M. M., Murulana L. C., Ozcan M., *Inter J. Electrochem. Sci.*, 7 (2012) 5035.

42. Elmsellem H., Karrouchi K., Aouniti A., Hammouti B., Radi S., Taoufik J., Ansar M., Dahmani M., Steli H., El Mahi B., *Der Pharma Chemica*, 7(10) (2015) 237-245.

43 El Belghiti M., Karzazi Y., Dafali A., Hammouti B., Bentiss F., Obot I. B., Bahadur I., Ebenso E. E., *J. Mol. Liq.* 218 (2016) 281-293.

44. Lahmidi S., Elmsellem H., Elyoussfi A., Sebbar N. K., Essassi E. M., Ouzidan Y., Kandri Rodi Y. , Dguigui K., El Mahi B and Hammouti B., *Der Pharma Chemica*, 8(1) (2016) 294-303.

45. El Mounsi I., Elmsellem H., Aouniti A., Bendaha H., Mimouni M., Benhadda T., Mouhoub R., El Mahi B., Salhi A and Hammouti B., *Der Pharma Chemica*. 7(10) (2015) 350-356.

(2016); http://www.jmaterenvironsci.com/